Neuron, Vol. 34, 905–919, June 13, 2002, Copyright ©2002 by Cell Press

A Long CAG Repeat in the Mouse *Sca1* Locus Replicates SCA1 Features and Reveals the Impact of Protein Solubility on Selective Neurodegeneration

Kei Watase,[1,5] Edwin J. Weeber,[2] Bisong Xu,[3] Barbara Antalffy,[3] Lisa Yuva-Paylor,[1] Kouichi Hashimoto,[6] Masanobu Kano,[6] Richard Atkinson,[1,4] Yaling Sun,[1] Dawna L. Armstrong,[3] J. David Sweatt,[2] Harry T. Orr,[7] Richard Paylor,[1,2] and Huda Y. Zoghbi[1,2,4,5,8]

[1]Department of Molecular and Human Genetics
[2]Division of Neuroscience
[3]Department of Pathology
[4]Department of Pediatrics
[5]Howard Hughes Medical Institute
Baylor College of Medicine
One Baylor Plaza
Houston, Texas 77030
[6]Department of Cellular Neurophysiology
Graduate School of Medical Science
Kanazawa University
13-1 Takara-machi
Kanazawa 920-8640
Japan
[7]Institute of Human Genetics
University of Minnesota
Mayo Mail Code 206
Minneapolis, Minnesota 55455

Summary

To faithfully recreate the features of the human neurodegenerative disease spinocerebellar ataxia type 1 (SCA1) in the mouse, we targeted 154 CAG repeats into the endogenous mouse locus. *Sca1*$^{154Q/2Q}$ mice developed a progressive neurological disorder that resembles human SCA1, featuring motor incoordination, cognitive deficits, wasting, and premature death, accompanied by Purkinje cell loss and age-related hippocampal synaptic dysfunction. Mutant ataxin-1 solubility varied with brain region, being most soluble in the neurons most vulnerable to degeneration. Solubility decreased overall as the mice aged; Purkinje cells, the most affected in SCA1, did not form aggregates of mutant protein until an advanced stage of disease. It appears that those neurons that cannot sequester the mutant protein efficiently and thereby curb its toxicity suffer the worst damage from polyglutamine-induced toxicity.

Introduction

Spinocerebellar ataxia type 1 (SCA1) is one of several dominantly inherited, late-onset neurodegenerative disorders caused by the expansion of a CAG trinucleotide repeat that encodes polyglutamine in the respective disease proteins. At least eight other disorders result from this pathogenic mechanism: spinobulbar muscular atrophy (SBMA), Huntington's disease (HD), dentatorubral pallidoluysian atrophy (DRPLA), and the spinocerebellar ataxias types 2, 3, 6, 7, and 17 (Zoghbi and Orr, 2000; Nakamura et al., 2001). The primary site of pathology varies somewhat from one disorder to the next, even though the respective disease-causing proteins are widely expressed; in SCA1, the mutant ataxin-1 protein causes degeneration predominantly of cerebellar Purkinje cells and neurons within the brain stem and spinal cord, producing a progressive ataxia and bulbar dysfunction that lead to death 15–20 years after the first appearance of symptoms (Zoghbi and Orr, 1995). In all the polyglutamine disorders, the length of the CAG repeat correlates directly with disease severity: the longer the repeat, the more severe the symptoms, and the earlier the age of onset. The polyglutamine expansion seems to confer on the proteins some toxic gain-of-function that intensifies with longer repeats, such that pathology is more widespread in juvenile-onset cases than in adult-onset patients. The mechanism by which a widely expressed, expanded polyglutamine tract leads to neurodegeneration of only certain neuronal groups remains elusive.

One of the most fruitful approaches to studying polyglutamine diseases has been to generate transgenic mouse models expressing truncated or full-length cDNAs encoding the mutant protein in neurons (review; Lin et al., 1999; Gusella and MacDonald, 2000). Most of these transgenic mice overexpress the mutant protein under either neuron-specific or ubiquitous promoters, which is enough to reproduce various aspects of the human neurological phenotypes, including aggregate formation in neurons. The role of these aggregates in the disease process has been controversial; although data suggest that the aggregates themselves are not necessary for initiating disease (Klement et al., 1998), their role in pathogenesis remains unclear, and much effort has been directed toward interventions that seek to eradicate these deposits.

To model SCA1, Burright et al. (1995) generated transgenic animals that overexpress mutant ataxin-1 transcripts under the control of the Purkinje cell *pcp2* promoter. One of these transgenic lines, the B05 line, expresses a full-length mutant ataxin-1 mRNA with 82 CAG repeats (82Q) at around 50–100 times endogenous levels in Purkinje cells after postnatal day (P)10 and develops the ataxia typical of human SCA1. These mice allowed the discovery that several specific genes are downregulated in Purkinje cells before any detectable pathological changes (Lin et al., 2000), which suggests that mutant ataxin-1 may initiate the disease process by altering gene expression. Studies of the B05 mice also provided early evidence that misfolding and impaired degradation of mutant ataxin-1 might underlie SCA1 pathogenesis (Cummings et al., 1998). This hypothesis was supported by recent studies showing that the disease phenotype of B05 mice was aggravated by dysfunction of the ubiquitin-proteasome (UPP) pathway (Cummings et al., 1999) but suppressed by overexpression of inducible Hsp70 chaperone (Cummings et al., 2001).

Although the B05 mice have been useful for disclosing

[8]Correspondence: hzoghbi@bcm.tmc.edu

disease mechanisms, they show only the phenotype associated with dysfunctional Purkinje cells and usually live a normal lifespan. This makes direct comparison with human SCA1 difficult, since human SCA1 patients develop cognitive impairment as the disease progresses, and the final stage of the disease is quite complex, causing patients to die early. In theory, a "knockin" approach, in which the human mutation is introduced into the corresponding mouse gene, should provide a more accurate genetic model. Expression from the endogenous locus should guarantee accurate temporal and spatial expression patterns at endogenous levels and help us dissect the mechanisms of cell-specific vulnerability or selective neurodegeneration. To this end, we generated knockin mice carrying 78 CAG repeats in the mouse *Sca1* locus (Lorenzetti et al., 2000). Although these *Sca1*$^{78Q/2Q}$ mice express expanded ataxin-1 at endogenous levels in a proper spatial and temporal pattern, they show only mild behavioral changes late in life. Hypothesizing that the short lifespan of the mouse does not allow sufficient time for its neurons to accumulate significant damage, we targeted an expanded repeat of 154 CAGs into the mouse locus. These *Sca1*$^{154Q/2Q}$ mice reproduced many aspects of the human disease and shed light on several aspects of polyglutamine-induced pathogenesis, including the relationship between aggregate formation and neuronal dysfunction.

Results

Generation of *Sca1*$^{154Q/2Q}$ Mice and Analysis of Mutant Protein

An expanded repeat of 154 CAGs was targeted into the mouse *Sca1* locus (*Sca1*^{154Q}) as previously described (Lorenzetti et al., 2000). Chimeric mice were generated by microinjection of correctly targeted ES cells into C57Bl/6J blastocysts and were mated to C57Bl/6J females (Figure 1A). Crosses between F1 mice carrying an *Sca1*^{154Q} allele produced wild-type, heterozygous, and homozygous offspring in expected proportions (data not shown).

Expression of the mutant transcript was assessed by RT-PCR using primers flanking the CAG repeat. Total RNA was extracted from a 7-week-old *Sca1*$^{154Q/2Q}$ mouse brain. As shown in Figure 1B, both mutant and wild-type transcripts produced almost equivalent band intensities, suggesting that mutant and wild-type alleles were similarly transcribed. The expression of mutant ataxin-1 was confirmed by Western analysis of mutant mouse brain extracts, which were prepared with 0.25 M Tris-containing buffer (Figure 1C). Surprisingly, in the adult mouse brain, the 11750 antibody, which was raised against the C-terminal portion of ataxin-1 (Servadio et al., 1995), recognized mutant ataxin-1 as a much fainter ~150 kDa band than its wild-type counterpart. This band also displayed immunoreactivity when the same blot was stripped and reprobed with 1C2 antibody, which detects long polyglutamine tracts. Neither 1C2, 11750, or the 11NQ antibody (which detects the N-terminal portion of ataxin-1) revealed any cleaved products derived from mutant ataxin-1.

To gain further insight into the apparent difference between levels of the wild-type and mutant protein in brain, we extracted proteins from mutant brains at three different ages and analyzed them by immunoblotting (Figure 1D). Although mutant ataxin-1 created a distinct, strong band in a 2-week-old mouse brain, it became fainter as the mice got older and was barely detectable at 25 weeks of age. This is not likely due to any age-dependent increase in mutant ataxin-1 degradation, since immunohistochemical analysis with 11NQ revealed dense staining, often with intranuclear inclusion formation, in various neuronal populations from 12-week-old *Sca1*$^{154Q/154Q}$ mouse brains (see also below). Rather, this difference in the densities of monomeric mutant and wild-type bands likely derives from differences in extraction or solubilization rather than actual levels of those proteins: the mutant protein accumulates into nuclear aggregates and becomes less extractable as mutant animals get older. In order to analyze aggregated forms of mutant ataxin-1 on immunoblot, we next utilized brain extracts prepared with urea/SDS-containing buffer. Brain extracts from mutants, but not control littermates, gave distinct ataxin-1 immunoreactivity (ATX-1 IR) in the top part of the stacking gels (Figure 1F). Densities of the ATX-1 IR got stronger as the mutants became older, indicating age-dependent increases in mutant ataxin-1 aggregation.

Since ataxin-1 is highly abundant in neurons, we also compared the expression and extractability of ataxin-1 among various brain regions of 3-week-old mice to see if there are any regional differences that could account for selective neuronal dysfunction or degeneration. As shown in Figure 1E, levels of wild-type ataxin-1 vary among brain sub-regions, with high levels in cerebral cortex, basal ganglia, hippocampus, and cerebellum. There are considerable differences in the extractability of mutant ataxin-1 in different brain regions. Mutant ataxin-1 gave fainter bands (i.e., was less extractable) in the basal ganglia and cerebral cortex than in the cerebellum, brain stem, spinal cord, and olfactory bulb.

Neurological Phenotype of *Sca1*$^{154Q/2Q}$ Mice

Up to 7 weeks of age, the mutant mice were indistinguishable from their wild-type littermates in home cage behavior. At 8 weeks of age, they began to show growth retardation. By 11 weeks of age, they weighed about 20% less than their wild-type littermates (Figure 2B). The body weight of the *Sca1*$^{154Q/2Q}$ mice peaked at around 20 weeks of age, after which the mice gradually lost weight as the disease progressed.

By the ninth week, the mutants started showing a clasping phenotype when suspended by the tail. The neurological phenotype progressed to a generalized muscle wasting, ataxia, and abnormal gait by 20 weeks of age. We observed severe kyphosis (curvature of the spine) accompanied by atrophy of lower limb muscles in the mutant animals at about 30 weeks (Figure 2A). Premature death occurred between 35 and 45 weeks of age (Figure 2D). None of the mutant animals survived past 50 weeks. The mice did not manifest any obvious seizures.

Naïve *Sca1*$^{154Q/2Q}$ mice were tested on the accelerating rotarod apparatus at 5 and 7 weeks of age (Figure 2C). Although they had no overt gait ataxia at that time, their

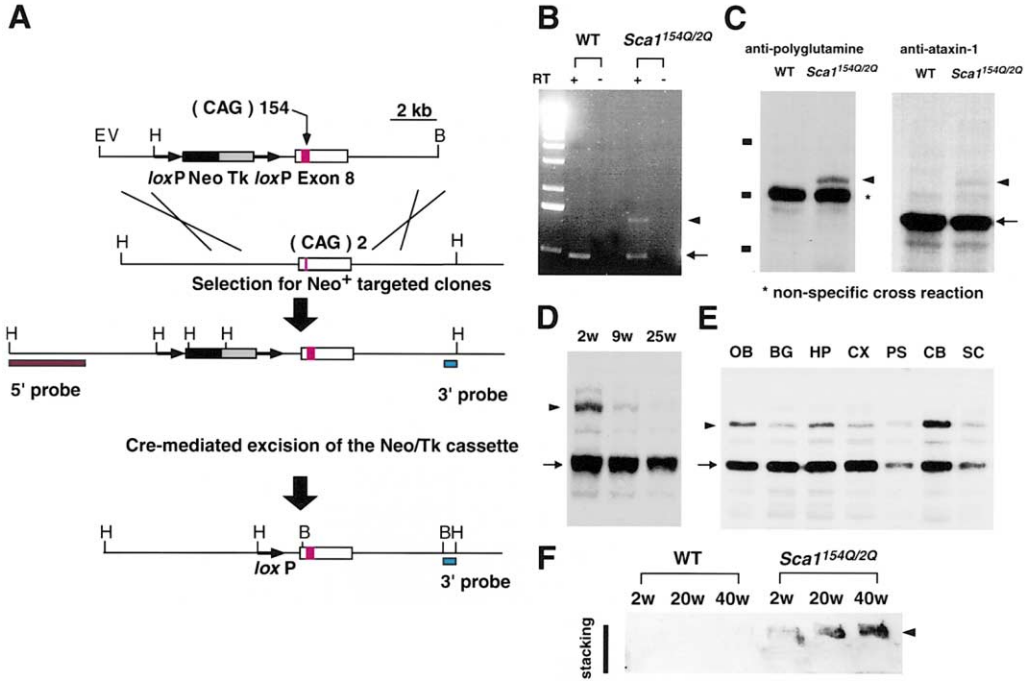

Figure 1. Generation and Expression of an Expanded CAG Allele at the *Sca1* Locus

(A) This schematic represents the targeting construct, the endogenous *Sca1* allele, and the predicted structure of the mutant CAG expansion allele generated by a homologous recombination and a Cre-mediated excision event.

(B) RT-PCR analysis was performed on brain RNA from a 7-week-old *Sca1*$^{154Q/2Q}$ knockin mouse (*Sca1*$^{154Q/2Q}$) and a wild-type littermate (wt) with (+) or without (−) reverse transcriptase. The forward primer is located in exon 7, while the reverse primer sits right after the CAG repeat sequence in exon 8. The reaction gives 968 bp for the wild-type allele (arrow) and 1421 bp for the *Sca1*^{154Q} allele (arrowhead).

(C) Western blot analysis was performed on whole brain extracts from a 7-week-old *Sca1*$^{154Q/2Q}$ knockin mouse (*Sca1*$^{154Q/2Q}$) and a wild-type littermate (wt), both probed with the 1C2 monoclonal antibody (left) and the 11750 antibody (right). Arrowhead and arrow indicate the mutant and wild-type ataxin-1 protein, respectively. The 1C2 antibody revealed nonspecific cross reactant (asterisk). Marker bands indicate 189, 119, and 85 kDa, respectively.

(D) Whole brain extracts (100 μg) from 2-, 9-, and 25-week-old *Sca1*$^{154Q/2Q}$ knockin mice show an age-dependent decrease in the detectability of mutant ataxin-1 on an immunoblot probed with the 11750 antibody. Arrowhead and arrow indicate the mutant and wild-type ataxin-1 protein, respectively.

(E) Western blot analysis of protein extracts (80 μg) from various parts of a 3-week-old *Sca1*$^{154Q/2Q}$ mouse brain display differential mutant protein solubility. Abbreviations are as follows: OB, olfactory bulb; BG, basal ganglia; HP, hippocampus; CX, cerebral cortex; PS, pons; CB, cerebellum; SC, spinal cord. Arrowhead and arrow indicate the mutant and wild-type ataxin-1 protein, respectively. Relative densities of upper bands (mutant ataxin-1) compared to lower bands (wild-type protein) are as follows: OB, 0.29; BG, 0.09; HP, 0.21; CX, 0.09; PS, 0.29; CB, 0.58; SC, 0.36.

(F) Aggregated ataxin-1 was detected on immunoblot using the 11NQ antibody is depicted. Brain homogenates (150 μg) from 2-, 20-, and 40-week-old *Sca1*$^{154Q/2Q}$ knockin mice (*Sca1*$^{154Q/2Q}$) and wild-type littermate (wt) were prepared in buffer containing urea/SDS and analyzed by SDS-PAGE.

performance was significantly poorer than that of age-matched wild-type littermates at both 5 and 7 weeks of age ($p < 0.0005$ and $p < 0.0001$, respectively).

Learning and Memory in *Sca1*$^{154Q/2Q}$ Mice

Since cognitive impairment is one of the clinical features of SCA1, we assayed the cognitive function of *Sca1*$^{154Q/2Q}$ mice. Spatial learning performance was assessed using the Morris water maze. Since *Sca1*$^{154Q/2Q}$ mutants have notable motor impairment, we tested a group of *Sca1*$^{154Q/2Q}$ mice at 7–8 weeks of age on a visible platform task in which the animals are required to find a slightly submerged fixed platform whose location is marked by a large proximal cue (see Experimental Procedures).

Overall, the *Sca1*$^{154Q/2Q}$ mutants took considerably longer to locate the platform than wild-type mice ($p = 0.000001$) (Figure 3A), but a genotype X trial interaction ($p = 0.000002$) indicates that the performance of the two genotypes was dependent on the trial number. *Sca1*$^{154Q/2Q}$ mutants took more time and swam a greater distance to find the platform during the early trials (i.e., in trial blocks 1–6, $p < 0.05$) but performed as well as wild-type mice on trial blocks 7 and 8 ($p = 0.21$) (Figures 3A and 3B). There was no overall difference ($p = 0.564$) in swim speed between *Sca1*$^{154Q/2Q}$ and wild-type mice (Figure 3C), suggesting that simple motor impairment was not interfering with the performance of the mutant mice on this test.

The hidden platform test measures the ability of an animal to learn the spatial relationship between extramaze cues and the platform. Performance is assessed by recording the time it takes to locate the platform during training and characterizing the search pattern during a probe trial that is given after training.

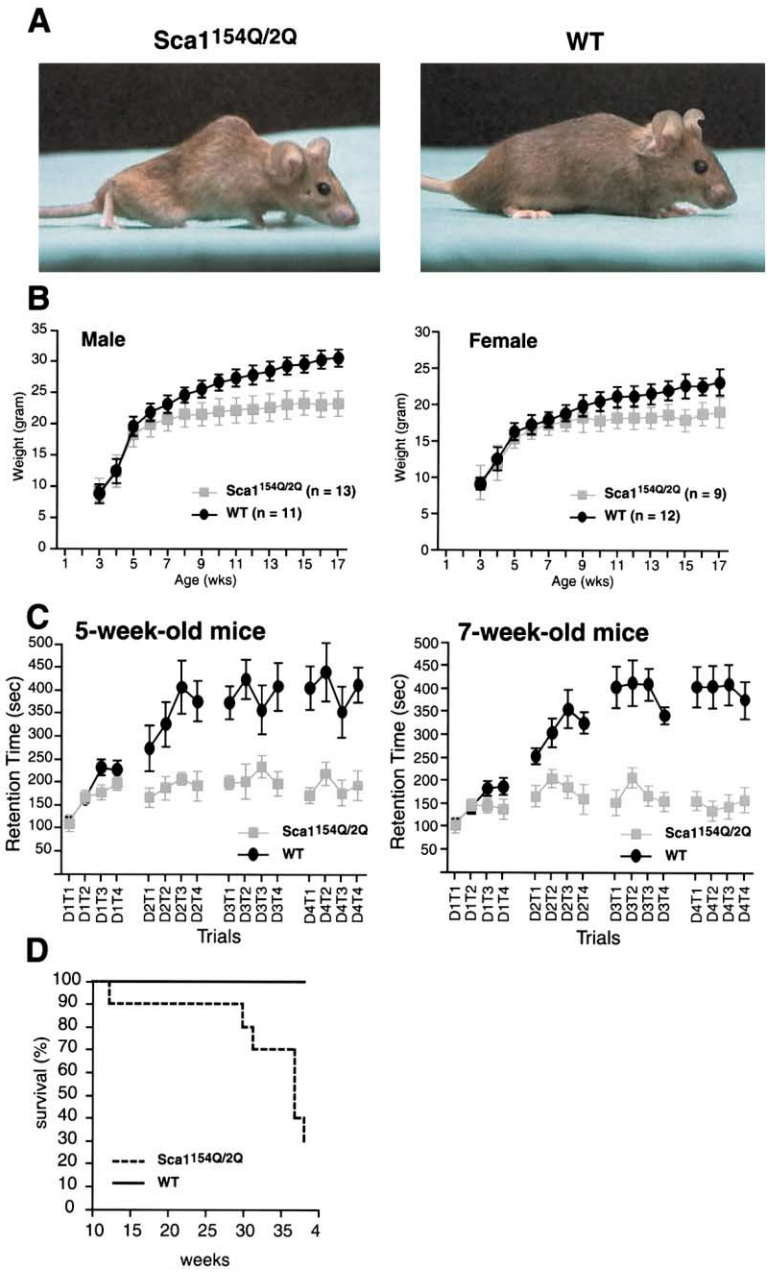

Figure 2. Phenotype of *Sca1*$^{154Q/2Q}$ Mice

(A) These photographs are representative of 28-week-old *Sca1*$^{154Q/2Q}$ mice and their wild-type littermates.

(B) *Sca1*$^{154Q/2Q}$ mice displayed progressive weight loss. Error bars indicate standard deviation.

(C) *Sca1*$^{154Q/2Q}$ mice showed impaired performance on the accelerating Rotarod apparatus. Performances of 5-week-old (left, n = 8 in each group) and 7-week-old (right, n = 10 in each group) mice are shown. Mice were trained in four trials per day (A–D) for 5 days (D1–D5). Naïve mutant mice and their wild-type littermates were tested in each test. Error bars indicate SEM.

(D) *Sca1*$^{154Q/2Q}$ mice had reduced lifespan. Percentage of *Sca1*$^{154Q/2Q}$ knockin (dashed line, n = 10) and wild-type (black line, n = 10) mice surviving at various ages is shown.

Sca1$^{154Q/2Q}$ mutant mice (at 7–9 weeks of age) took significantly more time (Figure 3D) to locate the hidden platform than wild-type mice ($p = 0.0000004$). Figures 3E and 3F show that during the probe trial, not only did wild-type mice spend significantly more time in the training quadrant than the *Sca1*$^{154Q/2Q}$ mutant mice ($p = 0.025$), but they also crossed the exact place where the platform had been located more often than *Sca1*$^{154Q/2Q}$ mutant mice ($p = 0.001$). These data indicate that *Sca1*$^{154Q/2Q}$ mice have impaired spatial learning performance.

The conditioned fear test assays Pavlovian learning and memory. Mice are placed in a test chamber (context) which they are allowed to explore freely. After 2 min, an auditory conditioned stimulus (CS) is presented and a mild footshock unconditioned stimulus (US) is delivered immediately upon termination of the auditory CS. The animals are presented a second CS-US pairing 2 min later. The mouse is then removed from the chamber and returned to its home cage; after a specified delay interval, the memory of the training experience is assessed using two test sessions (see Experimental Procedures). For the present study, 6- to 8-week-old *Sca1*$^{154Q/2Q}$ mutants and wild-type mice were trained and then tested either 1 hr or 24 hr later. The results from the context test (Figure 3G) show that there was a significant genotype X delay interval interaction ($p = 0.0436$). *Sca1*$^{154Q/2Q}$ mice displayed significantly less freezing than wild-type mice during the context test after a 24 hr delay ($p = 0.026$), but not after a 1 hr delay ($p = 0.883$). In contrast to the findings for the context test, there was no

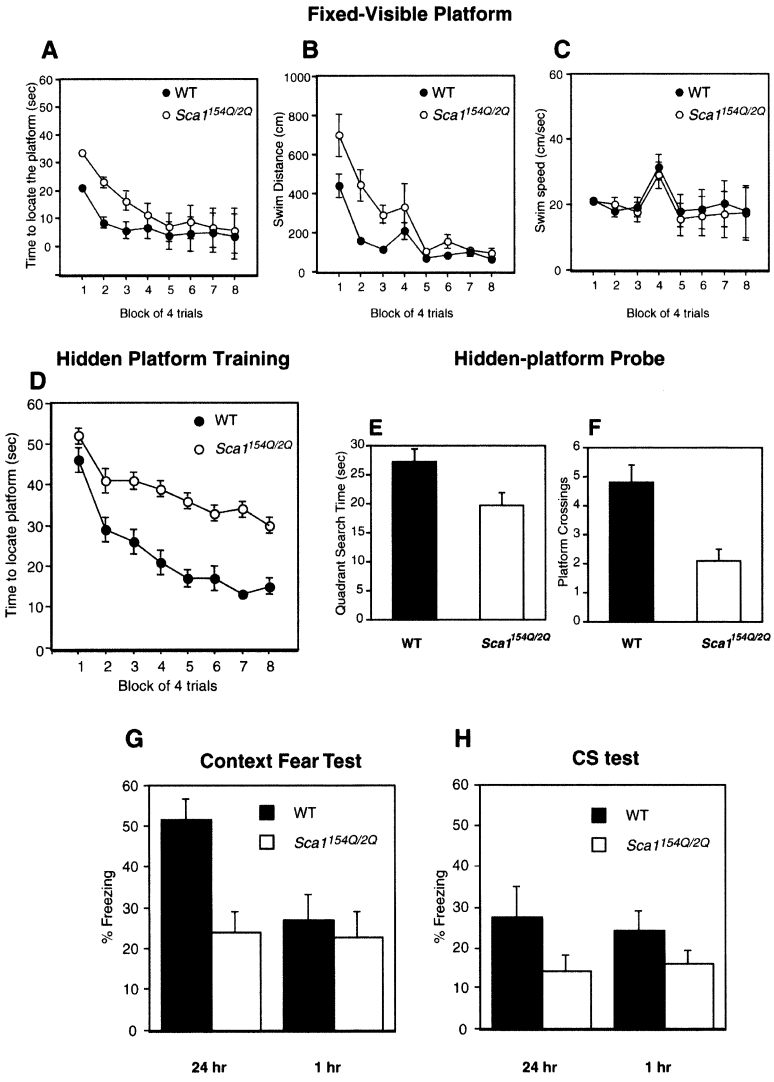

Figure 3. Impaired Learning and Memory in *Sca1*$^{154Q/2Q}$ Mice

(A and B) Latency (A) and distance (B) traveled to find the visible platform differed for *Sca1*$^{154Q/2Q}$ and wild-type (WT) mice. (C) indicates swim speed in the visible platform task for *Sca1*$^{154Q/2Q}$ and WT mice.

(D) Latency to find the hidden platform in the Morris water task for *Sca1*$^{154Q/2Q}$ and WT mice is shown. (E and F) This graph presents quadrant search time (E) and number of platform crossings for the training quadrant (F) after hidden platform training in the Morris water task for mutant and wild-type mice. (G) and (H) show Pavlovian conditioned fear for *Sca1*$^{154Q/2Q}$ and wild-type (WT) mice with percentage of intervals spent in freeze during the context test (F) and CS test (G). All data are expressed as the mean (±SEM).

genotype X delay interval interaction for the conditioned stimulus ($p = 0.687$) (Figure 3H). Thus, the difference between *Sca1*$^{154Q/2Q}$ and wild-type mice depends on the type of test (context versus CS) and the delay interval (24 hr versus 1 hr).

Hippocampal Synaptic Function in *Sca1*$^{154Q/2Q}$ Mice

It was previously shown that ataxin-1 is required for normal short-term synaptic plasticity in hippocampal CA1 neurons; ataxin-1 knockout mice displayed impaired paired pulse facilitation (Matilla et al., 1998). We hypothesized that the electrophysiological properties of CA1 neurons might be altered by a dominant-negative or gain-of-function mechanism in mutant ataxin-1. We therefore examined the effect of the mutation on the synaptic function of CA1 neurons using extracellular recordings from hippocampal slices. First, we tested hippocampal slices from 5-week-old animals. We observed no significant difference between 5-week-old *Sca1*$^{154Q/2Q}$ mice and wild-type controls in baseline synaptic transmission, paired pulse facilitation (PPF), or long-term potentiation (LTP) (Figures 4A and 4B).

A hallmark of polyglutamine disease is the appearance of neuronal intranuclear inclusions (NIs). No NIs were observed in 5-week-old mouse brains, but ubiquitinated NIs were abundant in CA1 hippocampal neurons at 7 weeks of age (see below). We therefore examined the electrophysiological responses of CA1 neurons at 8 weeks of age. Mutant animals had normal input-output functions, PPF, and LTP (Figures 4C and 4D), suggesting that NIs do not alter synaptic transmission or plasticity at this age. Older (24-week-old) *Sca1*$^{154Q/2Q}$ mice, however, exhibited a decrease in the input-output functions for stimulation of Schaffer collateral inputs into area CA1 (Figure 4E, $p < 0.02$), suggesting that basal synaptic transmission is impaired in the older *Sca1*$^{154Q/2Q}$ mutant hippocampus. The derangement in synaptic transmission manifested itself as an alteration in the pEPSP relative to fiber volley amplitude (Figure 4E). In addition, mutant slices exhibited a decrease in maximum EPSP response (Figures 4E and 4G).

Although derangement in baseline synaptic transmission may complicate evaluation, we proceeded to LTP analysis in the 24 week-old *Sca1*$^{154Q/2Q}$ mutants. Tetanic

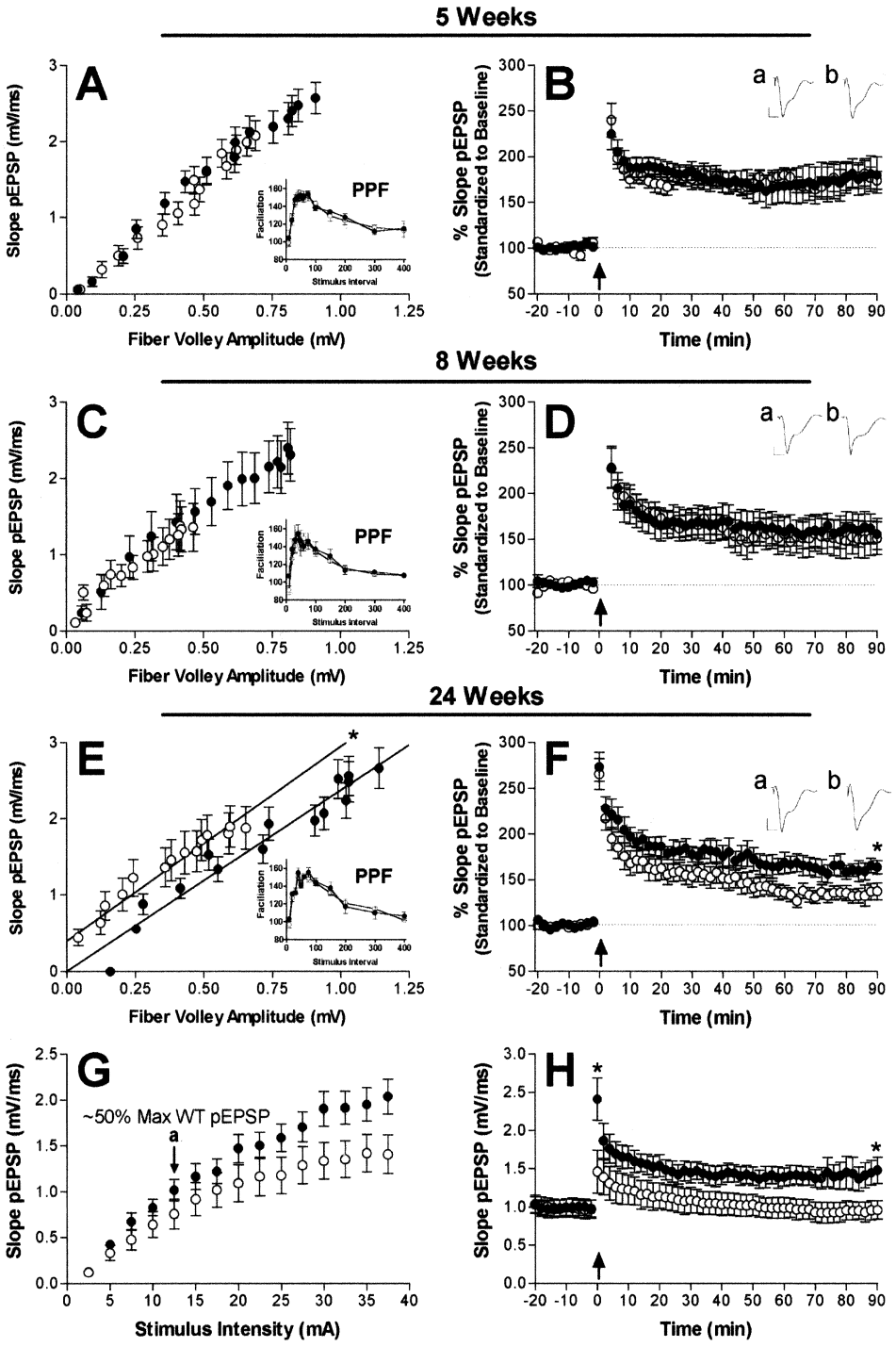

Figure 4. Effect of the Knockin Mutation on Hippocampal Physiologic Responses in Area CA1

Hippocampal slices obtained from *Sca1*$^{154Q/2Q}$ mice (open circle) or wild-type mice (closed circle) were utilized in experiments to evaluate baseline synaptic function and short- and long-term forms of synaptic plasticity. Baseline synaptic transmission was determined by analyzing the slope of the population excitatory postsynaptic potential (pEPSP) compared to the amplitude of the fiber volley. 5- and 8-week-old *Sca1*$^{154Q/2Q}$ mutants show no significant differences in synaptic transmission (A and C). Paired-pulse facilitation (PPF) was unaffected in all age groups tested: 5-, 8-, and 24-week-old Sca1$^{154Q/2Q}$ mutants (insets in [A], [C], and [E]). Derangement of synaptic transmission was seen in 24-week-old *Sca1*$^{154Q/2Q}$ mutants (E). Representative pEPSP traces (mean of six successive EPSPs) of baseline synaptic transmission for each age group are shown (insets in [B], [D], and [F]) (scale bars are 1 mV and 10 ms). Long-term potentiation (LTP) induced in stratum radiatum of area CA1 of the hippocampus using 100 Hz stimulation (indicated by an arrow) is normal in 5-week-old *Sca1*$^{154Q/2Q}$ animals (B) and 8-week-old *Sca1*$^{154Q/2Q}$ animals (D), but LTP was significantly reduced in 24-week-old mutants (90 min: WT 163 $\pm$ 7.4, n = 7 and *Sca1*$^{154Q/2Q}$ 137 $\pm$ 9.1, n = 9, p = 0.026) (F). Input-output curves were generated from 24-week-old *Sca1*$^{154Q/2Q}$ knockin mice by measuring the slope of the pEPSP at increasing stimulus intensities (G). (see a) The stimulus intensity needed to elicit 50% of the maximum pEPSP slope for wild-type animals was determined

stimulation in slices from the 24-week-old animals elicited normal post-tetanic potentiation (PTP), but a reduced potentiation was seen immediately following high-frequency stimulation (HFS). This diminution of potentiation lasted 90 min post-tetanus (Figure 4F).

Our usual LTP-induction protocol uses a stimulus intensity that elicits ~50% of the maximum pEPSP to evaluate both baseline synaptic transmission and the period of LTP-inducing, 100 Hz high-frequency stimulation. As shown in Figure 4G, the maximum pEPSP slope in 24-week-old mutants was considerably lower than that of the wild-type controls. In other words, beginning with a lower absolute EPSP magnitude, the *Sca1*$^{154Q/2Q}$ mutants achieved 50% of the maximum slope of the pEPSP and thus achieved a lower EPSP magnitude during LTP-inducing high-frequency stimulation. This could underlie the difference in *Sca1*$^{154Q/2Q}$ LTP induction, since the EPSP magnitude during stimulation could have an effect on the overall potentiation produced. Therefore, in our next set of experiments, we determined the stimulus intensity required to elicit 50% of the maximum pEPSP in our wild-type group (Figure 4G, arrow at a) and then adjusted the stimulus used in our *Sca1*$^{154Q/2Q}$ mutants to give a pEPSP with a similar EPSP slope (see baseline in Figure 4H). We found that the stimulus intensity required to give approximately equal pEPSPs (~950 mV/ms) was 12.5 and 17.5 mA for wild-type and *Sca1*$^{154Q/2Q}$ mutants, respectively. At the stated stimulus intensities, the recorded baseline pEPSPs were indistinguishable for both animal groups prior to high-frequency stimulation (HFS) (Figure 4H).

When the absolute pEPSP magnitude of control and knockin animals was compared, there was a significant decrease in the pEPSP magnitude in the mutant animals 90 min after HFS (Figure 4H, $p = 0.02$). Moreover, using the 17.5 mA stimulus intensity, the *Sca1*$^{154Q/2Q}$ mice showed a complete loss of potentiation to baseline levels by 30 min post-HFS. These results suggest that the hippocampal LTP deficit observed in the 24-week-old *Sca1*$^{154Q/2Q}$ mice reflects a deficit in HFS-dependent synaptic plasticity. It is important to note that for the second experiment, where EPSP magnitudes were comparable, the apparent deficit in LTP could be due to the CA1 Schaffer collateral synapse already being near the maximal response, which would manifest as an inability to reach an appreciable HFS-induced potentiation.

Electrophysiology of Purkinje Cells in Young *Sca1*$^{154Q/2Q}$ Mice

Sca1$^{154Q/2Q}$ mice developed motor incoordination at 5 weeks of age. At this stage, the Purkinje cells appeared grossly normal by calbindin immunofluorescence, though we could not rule out subtle changes in distal dendrites (see below). To probe the mechanism underlying impaired motor coordination in young mutant animals, we examined the electrophysiological properties of cerebellar Purkinje neurons at a relatively early age (6 to 11 weeks) using whole-cell recordings in cerebellar slices. We first compared passive membrane properties of Purkinje cells by recording membrane currents in response to hyperpolarizing voltage steps from the holding potential of −70 to −80 mV. As reported previously (Llano et al., 1991), the decay of the current was biphasic and could be described by the sum of two exponentials (data not shown). From their time constants, we calculated several parameters representing passive properties of Purkinje cells based on the model equivalent circuit of PCs described by Llano et al. (1991) (Table 1). This model distinguishes two regions in the Purkinje cell. Region 1 represents the soma and the main proximal dendrite; region 2 represents the main part of dendritic tree. The lumped membrane capacitance of regions 1 and 2 were calculated as C1 and C2, respectively. We found that the lumped membrane capacitance of the dendritic tree (C2) was significantly smaller in *Sca1*$^{154Q/2Q}$ mice than wild-type mice ($p < 0.01$, t test) (Table 1). Given the discernible reduction of dendritic arbor at advanced stages of disease, these results likely reflect a reduction in the average total membrane area of the dendritic tree in young *Sca1*$^{154Q/2Q}$ mice.

We then assessed the kinetics and short-term plasticity of climbing fiber-mediated (CF) and parallel fiber-mediated (PF) EPSCs. The decay time constant was obtained by fitting the decay phases of the EPSCs with single exponentials. We observed no significant difference between those young *Sca1*$^{154Q/2Q}$ mice and wild-type controls in the kinetics of the rise and decay times for both the CF- and PF-EPSCs (Table 1), paired-pulse facilitation of PF-EPSC, or in paired-pulse depression of CF-EPSC (data not shown). The degree of multiple climbing fiber innervation of Purkinje cells was similar between wild-type mice and *Sca1*$^{154Q/2Q}$ mice (data not shown). In addition, there was no significant difference between the two mouse strains in the chord conductance for CF-EPSCs (Table 1). These results suggest that synapse formation and function at this age are not altered in the mutant animals.

Nuclear Inclusions in Different Brain Regions

Immounohistochemical analysis of ataxin-1 in control adult mouse brains shows that ataxin-1 localizes predominantly to the nuclei of neurons throughout the nervous system. We detected neuronal NIs by immunohistochemistry in multiple neuronal populations in mutant brains. By light microscopic analysis, NIs were first evident as a single, small dot at 6 weeks of age in cortical neurons, CA1 hippocampal neurons, and thalamic nuclei. In end-stage brains, we observed large NIs with dense staining in these neurons. In addition, we observed inclusions within neurons in various other regions (caudate, putamen, cerebellum, brain stem, and spinal cord). Mapping of NIs in the mutant brains revealed

to be 12.5 mV (G, a), compared to 17.5 mV needed to elicit a pEPSP with a similar slope for *Sca1*$^{154Q/2Q}$ mice. With pEPSP slopes being equal, HFS-induced potentiation showed a significant reduction in *Sca1*$^{154Q/2Q}$ mice (H). The pEPSPs immediately following HFS were significantly reduced in *Sca1*$^{154Q/2Q}$ mutants (wt 2411 ± 277.0, $n = 7$ and *Sca1*$^{154Q/2Q}$ 460 ± 280.9, $n = 5$, $p = 0.02$) and were consistent for the duration of the experiment (90 min post-tetanus: wt 1481 ± 171.7, $n = 7$ and *Sca1*$^{154Q/2Q}$ 959 ± 120.4, $n = 5$, $p = 0.02$) (Data points and error bars represent the mean ± SEM).

Table 1. Electrophysiological Parameters of the Purkinje Cell

	Wild-Type	*Sca1*$^{154Q/2Q}$
[a]Passive membrane properties	n = 14	n = 16
C1 (pF)	184 ± 19	164 ± 16
C2 (pF)	1038 ± 60**	776 ± 50**
R1 (MΩ)	6.8 ± 0.3	6.6 ± 0.3
R2 (MΩ)	7.4 ± 0.5	8.4 ± 0.6
R (MΩ)	219.8 ± 22.0	408.4 ± 97.7
CF-EPSC	n = 24	n = 24
10%–90% rise time (ms)	0.4 ± 0.01	0.4 ± 0.01
[b]Decay time constant (ms)	5.4 ± 0.20	5.0 ± 0.24
[c]Chord conductance (nS)	111.6 ± 7.4	100.3 ± 11.4
PF-EPSC	n = 10	n = 8
10%–90% rise time (ms)	1.0 ± 0.04	1.0 ± 0.13
[b]Decay time constant (ms)	8.9 ± 0.93	8.5 ± 0.92

[a]Parameters for passive membrane properties were calculated according to the model described by Llano et al. (1991), which distinguishes two regions of Purkinje cells: region 1, which represents the soma and the main proximal dendrites, and region 2, which represents the dendritic tree. C1 and C2 represent the lumped membrane capacitance of regions 1 and 2, respectively. R1 represents the pipette access resistance. Region 2 is linked to region 1 by resistor R2, which represents the lumped resistance between the main proximal dendrite and each membrane region of the distal dendrites. R3 represents the lumped resistance of the dendritic tree of PCs. The values of C1, C2, R1, and R2 were calculated from the inital capacitive currents in response to hyperpolarizing voltage steps (500 ms duration) from −70 to −80 mV. The value of R3 was measured from the steady state currents in response to hyperpolarizing voltage steps (500 ms duration) from −80 to −85 mV.

[b]Decay time constants for CF- and PF-EPSCs were measured by fitting the EPSC decay with a single exponential. Holding potential was −80 mV.

[c]Chord conductance was measured from CF-EPSCs recorded at the holding potentials of −20 mV and +40 mV.

All data are expressed as mean ± SEM.

**$p < 0.01$ (t test).

considerable differences between neuronal groups in the appearance and abundance of NIs. For example, neither hypothalamic or cerebellar granule neurons develop NIs, but this is not surprising because ataxin-1 is expressed at very low levels in these neurons. Since it is known that in SCA1, marked neurodegeneration occurs in specific areas (Purkinje cells, red nucleus, olivary complex, and motor neurons in the anterior horn), we examined NI formation in the analogous mouse neurons to examine the relationship between NIs and neurodegeneration. Interestingly, we detected NIs less frequently in these most susceptible neuronal groups than in cortical or hippocampal pyramidal neurons, which show only mild neurodegeneration in SCA1 patient tissue (Figure 5). Less than 0.5% of Purkinje cells harbored tiny NIs before 20 weeks of age, while more than 80% of the neurons in the cerebral cortex and hippocampus contained NIs at the same age.

NIs in the knockin mice stained positive for ubiquitin (Figure 5M), as they do in B05 mouse and human tissue. Antibodies to HDJ2 chaperone failed to reveal any NIs in 7-week-old-brains, merely diffusely staining the cytoplasm (Figure 5N). As the NIs grow over time, some of NIs in the mutant hippocampus, cortex, and inferior olive become positive for HDJ2 by 18 weeks of age. In mutant brains from 40 weeks of age, most of the NIs in those areas (but not those in Purkinje cells) were recognized by the antibodies. Hsc70, which was also detected in ataxin-1 nuclear aggregates in Purkinje cells of B05 mice, was observed in most hippocampal or cortical NIs in 40-week-old, but not 7-week-old, mutant brains (data not shown). These results suggest that the involvement of HDJ2 chaperone as well as Hsc70 in NI may be secondary to the initial formation of NI or sequestration of ubiquitin. Alternatively, during the initial phase of NI formation, these chaperone proteins may be in a complex in the NI that might allow only limited access to antibodies.

In several other polyglutamine diseases, CREB binding protein (CBP) has been found to be sequestered into NIs, and interference of CBP-mediated transcription may be involved in neuronal toxicity (McCampbell et al., 2000; Nucifora et al., 2001). We stained brain sections derived from 7-, 20-, and 40-week-old *Sca1*$^{154Q/2Q}$ mice with two antibodies, A-22 and C-20 (Santa Cruz, CA), that recognize either the amino- or carboxyl-terminus of the protein. Although the CBP-IR was largely restricted to the nucleus, none of the ataxin-1 NIs were stained with them (data not shown).

Neuropathology of *Sca1*$^{154Q/2Q}$ Mice

We examined several mutant and wild-type mouse brains from different age groups, ranging from 4 weeks (juvenile) to 42 weeks (end-stage). Juvenile mutant mice showed no gross abnormalities, but brains from end-stage mutants were consistently smaller than those from littermate controls. 16-week-old mutants had significantly reduced brain weight ($p < 0.00002$ by ANOVA, Figure 6E). Brain sections obtained from the aged mice (40 weeks) showed uniform atrophy, with dilatation of all the ventricles (Figure 6F).

Inspection with anti-calbindin immunofluorescence uncovered no gross pathological changes in Purkinje cells from 17-week-old *Sca1*$^{154Q/2Q}$ mice (data not shown). Using quantitative analysis, however, on cerebellar slices from the 19-week-old animals (see Experimental Procedures), we found that wild-type Purkinje cells had dendritic arbors with approximately 50% higher fluorescence than their mutant counterparts (Figure 6G). Similar alterations were noted on slices from a pair of 9-week-old animals (data not shown). The lower fluorescence

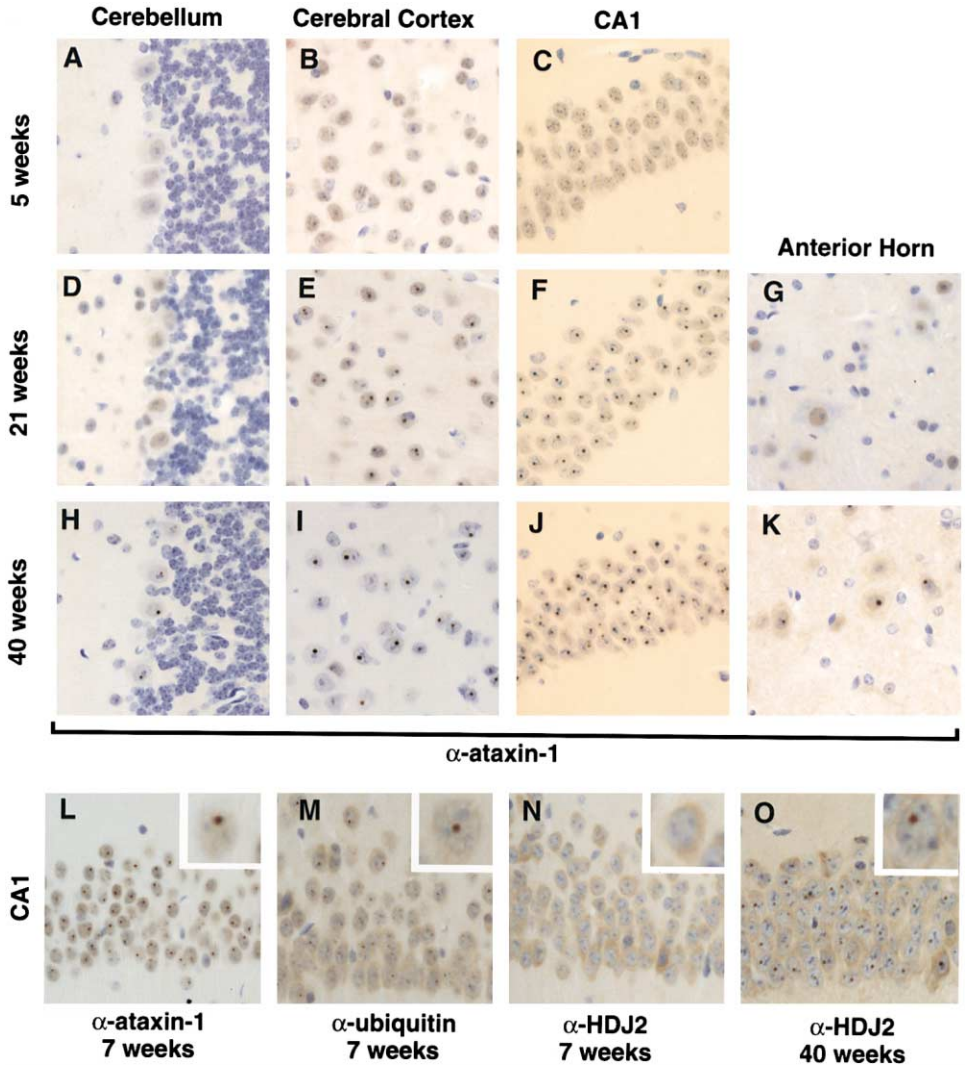

Figure 5. Characterization of NIs in *Sca1*$^{154Q/2Q}$ Brains

(A–K) NI distributions in *Sca1*$^{154Q/2Q}$ brains show temporal and regional patterns. Paraffin sections from cerebellar cortex (A, D, and H), cerebral cortex (B, E, and I), CA1 hippocampus (C, F, and J), and anterior horn of spinal cord (G and K) were stained with anti-ataxin-1 antibody 11NQ. Brains were collected at 5 (A–C), 21 (D–G), and 40 (H–K) weeks of age. Inclusions appear later in anterior horn neurons and Purkinje cells than in cortical neurons and hippocampal CA1 neurons. (L–O) NIs were revealed in CA1 hippocampal neurons of 7-week-old *Sca1*$^{154Q/2Q}$ mice by anti-ataxin-1 antibody 11NQ (L) or anti-ubiquitin antibody (M), but not by anti-HDJ-2 antibody (N). In a 40-week-old mutant's brain, most of the CA1 neurons possessed NIs stained with anti-HDJ-2 antibody (O). Insets show individual CA1 neurons at higher magnification. Original magnification for each photograph was 200×.

in mutant Purkinje cells indicates the paucity of fine dendritic arbor.

By 34 weeks of age, dendritic arborization was obviously reduced in cerebella from mutant animals (Figures 6A–6D) and Purkinje cell loss was noticeable. We quantified cell loss among Purkinje neurons and hippocampal pyramidal neurons on midsaggital sections stained with haematoxylin and eosin (HE) in 40-week-old mutants and their littermates. There were significantly ($p < 0.01$) fewer Purkinje neurons in the mutant cerebella (wild-type; 255.3 ± 9.4, *Sca1*$^{154Q/2Q}$ mice; 196.8 ± 11.6, mean ± SEM, per section; $n = 4$ animals). The relatively intact population of hippocampal pyramidal neurons in the mutant brains (wild-type; 497.3 ± 12.3, *Sca1*$^{154Q/2Q}$ mice; 461.7 ± 34.2, mean ± SEM, per section; $n = 3$ animals) underscores the greater vulnerablility of Purkinje neurons to mutant ataxin-1 toxicity. Purkinje cell loss did not appear to result from apoptotic mechanisms, based on negative Tunel staining (data not shown). Reactive astrocytosis was detected in the spinal cord by glial fibrillary acidic protein (GFAP) immunoreactivity; staining was most intense in the dorsal columns, but we also observed enhanced immunoreactivity in the ventral part, including the anterior horn. There was no increase in GFAP staining in other brain regions such as the cerebellum and brain stem.

Discussion

Sca1$^{154Q/2Q}$ mice develop a devastating neurological disease remarkably reminiscent of SCA1. Like SCA1 patients, *Sca1*$^{154Q/2Q}$ mice develop a complex, slowly pro-

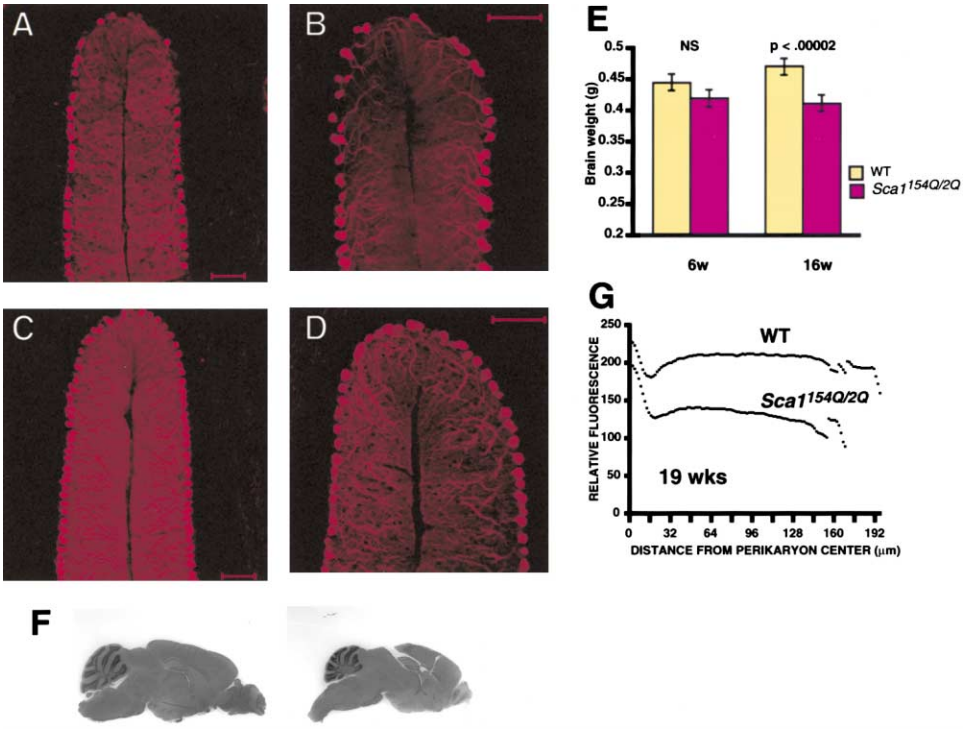

Figure 6. Neurodegenerative and Atrophic Changes in *Sca1*$^{154Q/2Q}$ Brains

(A–D) Immunofluorescence confocal microscopy of 34-week-old *Sca1*$^{154Q/2Q}$ mouse (A and B) shows altered cerebellar morphology (compared with wild-type mouse in [C] and [D]). Staining was performed with antisera against calbindin. Scale bars indicate 100 μm. (E) At 16 weeks, *Sca1*$^{154Q/2Q}$ mice showed a statistically significant reduction in brain weight compared to wild-type littermates. Error bars indicate SEM. (F) Mid-sagittal sections from the mutant and wild-type brains (40-week-old) highlight marked atrophy in the mutants. (G) Calbindin immunofluorescence obtained from selected rectangular subsections of wild-type or the mutant cerebella was quantified and averaged (n = 6, in each group). Calbindin immunofluorescence was reduced in 19-week-old *Sca1*$^{154Q/2Q}$ mice.

gressive neurodegeneration. Motor incoordination is apparent as early as 5 weeks of age on the rotarod test and later becomes frank gait ataxia. Human SCA1 patients display mild cognitive dysfunction, including reduction in recent and remote memory (Kish et al., 1988; Bürk et al., 2001); *Sca1*$^{154Q/2Q}$ mice show deficits in memory. The *Sca1*$^{154Q/2Q}$ mice also suffer muscle wasting, loss of body weight, and premature death—again, like human patients. Although body weight loss is associated with bulbar dysfunction (which causes difficulty in eating) in most human patients, some individuals undergo weight loss and wasting that is not attributable to dysphagia or modifiable by diet (Genis et al., 1995). It is possible that brain stem dysfunction contributes to body weight loss and premature death in *Sca1*$^{154Q/2Q}$ mice, but detailed studies are necessary to reach a conclusion on this point.

Having succeeded in developing a mouse model that invokes the correct temporal and spatial expression of the disease-causing mutation, some of the pathogenic questions that are specific to SCA1 and the polyglutamine diseases—e.g., selective neuronal vulnerability, role of inclusions in the disease process—can begin to be addressed.

Learning Deficits and Age-Dependent Impairment of Hippocampal Synaptic Transmission in *Sca1*$^{154Q/2Q}$ Mice

Mice with hippocampal dysfunction have been shown to have impaired context-based, but not cued, conditioned fear (Frankland et al.,1998; Logue et al.,1997; Jiang et al.,1998) and impaired spatial learning in the hidden-platform version of the Morris water task (Logue et al., 1997). The pattern of poor performance for the *Sca1*$^{154Q/2Q}$ mutants on the learning and memory tasks is consistent with altered hippocampal function and, indeed, *Sca1*$^{154Q/2Q}$ knockin animals exhibited an age-dependent derangement of hippocampal synaptic physiology. 5- and 8-week-old animals displayed normal baseline synaptic transmission, normal PPF, and normal LTP, but 24-week-old animals exhibited two alterations in baseline synaptic function. First, there was a significant leftward shift of the fiber volley-EPSP relationship for baseline synaptic transmission, which we take to indicate altered stimulus-response function for synaptic transmission in hippocampal area CA1—specifically, either an enhanced postsynaptic threshold responsiveness or an augmented baseline presynaptic neurotransmitter release. The normal PPF in these same slices might suggest that the presynaptic side of the terminal is not the site of change, as PPF is generally held to be a presynaptic phenomenon, but this evidence is by no means conclusive.

The second change we observed was a decrease in the maximum pEPSP slope in the mutant animals along with an apparent attenuation of LTP. Interpretation of the deficit in LTP is complicated by the fact that there was altered baseline synaptic transmission as described above, and a decrease in the maximum EPSP slope that could be evoked with physiologic stimulation. Neverthe-

less, LTP was diminished even when baseline transmission was normalized to 50% of the maximum and stimulus intensity was normalized so that both wild-type and knockin animals evoked the same absolute EPSP slope. We interpret our findings to indicate that there is altered LTP in *Sca1*$^{154Q/2Q}$ animals, with the important caveat that these apparent changes are superimposed on an altered baseline synaptic response. Overall, our observation of altered hippocampal synaptic physiology in the knockin animals complements our observation of altered hippocampus-dependent learning and memory in these animals.

Neuropathology in *Sca1*$^{154Q/2Q}$ Mice

Reduced dendritic arborization of Purkinje neurons was noted early in the course of disease in the knockin mice; Purkinje cell loss, though significant ($\sim$20%), did not occur until the end-stage of disease. Other neuronal groups we studied, such as the hippocampal neurons, suffered dysfunction while not revealing notable cell loss. This correlates with human data, since neuronal dysfunction goes on for many years before cell loss is a significant problem. In humans, cell loss is most prominent in Purkinje cells (the first neurons to become impaired), whereas hippocampal and cortical neuron loss is minimal, despite the fact that these patients suffer cognitive deficits (Zoghbi and Orr, 1995).

Polyglutamine-induced pathology in *SCA1* transgenic (B05) mice is characterized by cytoplasmic vacuoles, progressive loss of dendritic arborization, and Purkinje cell heterotopia (Clark et al., 1997). The combination of Purkinje cell heterotopia and cytoplasmic vacuole formation is unique to the transgenic mice and has not been observed in tissues from SCA1 patients; as well, our *Sca1*$^{154Q/2Q}$ mice do not display these features. These morphological differences suggest that the mechanism of Purkinje cell degeneration is not entirely the same in the two models, which differ in both repeat length and mutant ataxin-1 expression levels. Since vacuole formation has been described for several in vitro overexpression models of polyglutamine disease, it may emerge only when neurons or cells are overloaded with polyglutamine proteins.

NI Formation, Ataxin-1 Extractability, and Neuronal Vulnerability

The tissue distribution of NIs in *Sca1*$^{154Q/2Q}$ mice is consistent with previous reports that NI formation does not initiate disease in SCA1 transgenic animals (Klement et al., 1998). NIs were rare and appeared only very late in the course of the disease in the mutant Purkinje neurons and spinal cord neurons, where we found the worst neurodegenerative pathology. On the other hand, NIs already populated most neurons of the cerebral cortex, CA1 hippocampus, and thalamus by the time mice reached 21 weeks of age. This is reminiscent of the neuropathology of a juvenile SCA1 patient in whom NI formation was detected in pontine neurons and some cortical neurons, but not in other areas, such as remaining Purkinje neurons (H.Y.Z., unpublished data). In a study of tissue from patients with Huntington's disease, Kuemmerle et al. (1999) also showed that inclusions form more frequently in nonaffected neuronal populations.

Interestingly, we found both temporal and regional alterations in mutant ataxin-1 extractability, which declines as the animals get older. The densities of the mutant and wild-type ataxin-1 were unequal even in 2-week-old brain extracts. It is noteworthy that the extractability of mutant ataxin-1 was higher in the cerebellum than the cerebral cortex and basal ganglia. In the cerebellum, ataxin-1 is expressed in various types of neurons, but immunfluorescence analysis indicated that its expression in granule neurons is much lower than that in Purkinje neurons (data not shown). This finding led us to propose that the extractable portion of the mutant protein in the cerebellum derived mainly from Purkinje cells.

An obvious pattern emerges from consideration of the earliest behavioral manifestations (impaired motor coordination), degrees of protein extractability (greatest in cerebellar tissue), electrophysiological changes (early, in Purkinje cells), sites of neurodegeneration (most notable in Purkinje cells), and NI formation (late, in Purkinje cells): neurons that sequester ataxin-1 into NIs only late in the course of the disease are also the cells that are most severely affected by polyglutamine toxicity. This finding is consistent with earlier studies on SCA1 transgenic mice showing that ataxin-1 toxicity was much greater when it was *not* sequestered in NIs (Cummings et al., 1999). NIs appear in vulnerable neurons at an early stage in SCA1 transgenic mice, most likely due to the very high expression of the mutant protein ($\sim$50$\times$ endogenous levels). Their relative absence in the most vulnerable neurons in human patients as well as the *Sca1*$^{154Q/2Q}$ mice suggests that the selective neuropathology in polyglutamine diseases reflects a complex combination of mutant protein expression levels, protein solubility, and the presence of factors that enable neurons to sequester ataxin-1 into NIs and thereby curb its toxicity.

This hypothesis is supported by recent findings on the pathophysiology of Alzheimer's disease (AD) and of Parkinson's disease (PD). A hallmark of pathology in both disorders is the presence of hard-to-solubilize, ubiquitin-positive deposits (senile plaques and Lewy bodies, respectively). But it is the soluble, not insoluble, pool of Aβ that correlates with neurodegeneration in AD (McLean et al., 1999). More recently, Walsh and colleagues (2002) demonstrated that it is the soluble oligomer form of Aβ that impairs hippocampal synaptic plasticity. The situation is similar in PD: mutations of parkin cause early-onset autosomal recessive PD characterized by the absence of Lewy bodies (Shimura et al., 2001). Shimura suggested that mutant parkin leads to the accumulation of a soluble, nonubiquitinated form of α-synuclein in parkin-deficient PD brains, accelerating neuronal loss and causing the earlier disease onset.

Factors in Polyglutamine Disease Pathogenesis

The phenotypic variability among human SCA1 patients and, indeed, among patients with other polyglutamine neurodegenerative diseases is notorious. Juvenile-onset cases display a widespread neuropathology that affects many regions besides the spinocerebellar system, they have more severe muscle wasting, and their symptoms progress much more rapidly than in adult-onset disease. Interestingly, Purkinje cell loss is less

prominent in juvenile cases, probably because there is insufficient time for this end-stage event to develop. To our knowledge, 82 repeats are the most that have been found in a human SCA1 patient (who developed disease at the age of 4 years).

Our results show that endogenous levels of mutant ataxin-1 can cause neurodegenerative disease during the short life-span of the mouse if the expanded polyglutamine tract is sufficiently long. Some aspects of the pathology differ slightly from those seen in adult-onset cases: the knockin mice develop inclusions in more brain regions than typically seen in humans. Nevertheless, this is consistent with the observation in SCA1 and other polyglutamine diseases that longer repeats produce earlier and much more severe disease, with far more widespread pathology. We strongly suspect that a human SCA1 patient with 154 repeats would display an infantile-onset disease, as has been observed in SCA7 patients with extremely long CAG tracts (Zoghbi and Orr, 2000). Homologous recombination has been used to introduce a similar length polyglutamine tract, ~150 CAG repeats, into the murine *Hdh locus* (Lin et al., 2001) in an effort to duplicate HD in the mouse, but Hdh^{150} mice failed to develop overt neurodegenerative disease. This strongly suggests that the protein context of the polyglutamine tract modulates the toxicity of the repeat, as we have suspected from human data: huntingtin with 120 CAG repeats has caused neurological abnormality at 5 years of age (Telenius et al., 1993) in a human child, while, as noted above, only 82 CAG repeats in ataxin-1 were required to cause symptoms in a human 4-year-old. Thus, protein levels, spatial and temporal distribution, protein context, and length of the polyglutamine tract are all crucial determining factors of polyglutamine-induced pathogenesis.

One difference between the transgenic and knockin mouse models is in the stage at which NIs develop in Purkinje cells and the redistribution of chaperones to those NIs. In the overexpression model, both events occur quite early in pathogenesis; massive overexpression may mount a strong heat shock response in the transgenic mouse cells, allowing early redistribution of chaperones to the site of mutant polyglutamine protein. In the knockin model, where the chaperones colocalize to the NIs late, the physiologic levels of the mutant protein may promote a much milder heat shock response.

What sequesters mutant ataxin-1 in NIs in various neuronal groups? Factors that help process the mutant proteins for ubiquitination or clearance may be more abundant in such neurons; proteins that modify ataxin-1 may be rate-limiting. Molecular chaperones might play a role since they are known to refold or enhance clearance of misfolded proteins. But, although Cummings et al. (2001) reported that overexpression of ihsp70 improves neuropathology in SCA1 transgenic mice, the mechanism by which this happens was not established; neither mutant ataxin-1 solubility nor abundance of NIs was affected. Microtubule- or cytoskeleon-associated molecules could also play a role in NI formation since disruption of the microtubule cytoskeleton leads to suppression of NI formation and enhancement of polyglutamine toxicity in yeast expressing a mutant huntingtin polypeptide (Muchowski et al., 2002). At this time, the factors contributing to the differential pattern of NI formation in this *Sca1* knockin model are not known, but future cross-species studies taking advantage of modifiers in the *Drosophila* SCA1 model (Fernandez-Funez et al., 2000) might help us identify such factors.

This knockin mouse replicates numerous aspects of the human disease, from progressive motor degeneration to selective neuronal vulnerability and cognitive deficits. Not only will this model allow us to study the mechanism of these varied deficits (particularly the special vulnerability of certain groups of neurons to triplet repeat toxicity) in vivo, but it provides a more authentic means of testing interventional therapies. These mice can be used, for example, to test the efficacy of compounds that have proven effective in other model organisms on multiple facets of the SCA1 phenotype (Steffan et al., 2001).

Experimental Procedures

Generation of $Sca1^{154Q/2Q}$ Mice

A targeting construct with 154 CAG repeats was prepared by culturing the SURE *E. coli* strain (Strategene) transfected with the bacterial plasmid vector previously made for generating $Sca1^{78Q/2Q}$ mice. The obtained plasmids were checked for the entire exon 8 of the *Sca1* gene by sequencing and then electroporated into ES cells derived from 129Sv/Ev strain (AB2.2). Homologous recombination was confirmed by Southern analysis as previously described (Lorenzetti et al., 2000). Chimeric mice were crossed with C57Bl6J females. F1 and F2 animals are used for the studies. Both male and female F2 animals obtained from crosses between F1 heterozygous males and C57Bl6J wild-type females were used for behavioral and neurophysiological studies.

Protein Expression and Extraction Analysis

Brain homogenates from each genotype were prepared by homogenizing either whole brain or specific subregions in 0.25 M Tris (pH 7.5) containing Complete (Roche) proteinase inhibitors. After homogenization, samples were briefly spun at 2500 rpm on the microcentrifuge (600 g), and supernatant was used for immunoblotting. For detection of aggregated forms of ataxin-1, samples were lysed in buffer containing 8 M urea, 4% SDS, 0.125 M Tris-HCl (pH 6.8), 12 mM EDTA, 3% β-mercaptoethanol, the proteinase inhibitor, and 0.002% bromophenol blue; incubated at 65°C for 10 min; and subjected to SDS-PAGE. Western blot analysis was performed as previously described (Skinner et al., 1997). Nitrocellulose blots were probed with polyclonal anti-ataxin-1 (11750VII, 1:3000, 11NQ, 1:3000) and monoclonal anti polyglutamine (1C2, 1:20000) antibodies.

Rotarod Analysis

An accelerated rotating rod test allowed us to evaluate coordination and motor skill acquisition (type 7650; Ugo Basile, Milan, Italy). Naïve F2 animals at 5 and 7 weeks of age were placed on the rod (3 cm diameter, 30 cm long) in four trials every day for a period of 4 days. Each trial lasted 10 min. The rod accelerated from 4 to 40 rpm in 5 min. The time the mice spent on the rod without falling was recorded. Behavioral scores were subjected to statistical analysis using ANOVA with repeated measures.

Visible Platform Test

7- to 8-week-old mice were trained on the visible platform test using the same procedures as those described for the hidden-platform test, with the exception that a black cube (7.5 cm × 7.5 cm) was attached to the top of the escape platform. The bottom of the block was 10 cm above the surface of the platform. The platform was located in the same place on each trial. Mice were given eight trials a day, divided into two blocks of four trials each, on 4 consecutive days. Following the last trial, the platform was removed and a 60 s probe trial was administered.

Pavlovian Conditioned Fear

Mice were 6–8 weeks old at the start of testing. Performance in a conditioned fear paradigm was measured as described before (Paylor et al., 1994) using a Freeze Monitor system (San Diego Instruments). The test chamber was made of clear Plexiglas and surrounded by a photobeam detection system. The floor of the test chamber was a grid used to deliver an electric shock. The test chamber was placed inside a sound-attenuated chamber (Med Associates); in the front of the chamber were windows through which the mice can be observed. A mouse was placed in the test chamber (house lights "ON") and allowed to explore freely for 2 min. A white noise (80 dB), which served as the conditioned stimulus (CS), was then presented for 30 s followed by a mild (2 s, 0.5 mA) foot-shock (the unconditioned stimulus,US). Two min. later another CS-US pairing was presented. The mouse was removed from the chamber 15–30 s later and returned to its home cage. Freezing behavior was recorded using the standard interval sampling procedure every 10 s. Responses (run, jump, and vocalize) to the foot-shock were recorded. Animals that did not respond to the footshock were excluded from analysis.

After a defined delay interval (24 hr for Experiment 1 and 1 hr for Experiment 2), the mouse was placed back into the test chamber for 5 min and freezing behavior was assessed every 10 s (context test). One to two hours later, the mouse was tested for its freezing to the auditory C. Environmental and contextual cues were changed for the auditory CS test: a black plexiglass triangular insert was placed in the chamber to alter its shape and spatial cues, red house lights replaced the white house lights, the wire grid floor was covered with black plexiglass, and vanilla extract was placed in the chamber to alter the smell. Finally, the sound attenuated chamber was illuminated with red house lights. There were two phases during the auditory CS test. In the first phase (pre-CS), freezing was recorded for 3 min without the auditory CS. In the second phase, the auditory CS was turned on and freezing was recorded for another 3 min. The number of freezing intervals was converted to a percentage of the freezing value. For the auditory CS test, the percentage freezing value obtained during the pre-CS period was subtracted from the percentage freezing value when the auditory CS was present.

Spatial Learning in the Morris Water Task

2 weeks after the conditioned fear test, mice were trained in the Morris water task to locate a hidden escape platform in a circular pool (1.38 min diameter) of water. Mouse performance was recorded using a tracking system called Noldus EthoVision (Leesburg, VA). Each mouse was given 8 trials per day, in blocks of four trials for 4 consecutive days. The time taken to locate the escape platform (escape latency) and the distance traveled were determined. After trial 32, each animal was given a probe trial. During the probe trial, the platform was removed and each animal was allowed 60 s to search the pool. The amount of time that each animal spent in each quadrant was recorded (quadrant search time). The number of times a subject crossed the exact location of the platform during training was determined and compared with crossings of the equivalent location in each of the other quadrants (platform crossing). Selective search data in the probe trial were analyzed by individual one-way (quadrants) repeated ANOVAs and Newman-Keuls post-hoc comparison tests. Two-way (genotype X gender) ANOVA was used to compare the quadrant search time and platform crossing data for the training quadrant only between mutant and wild-type mice.

Hippocampal Slice Physiology

Hippocampal slices (400 μm) were prepared from either 5-, 8-, or 24-week-old *Sca1*$^{154Q/2Q}$ mice and age-matched controls, as previously described (Roberson and Sweatt, 1996). Slices were perfused (1 ml/min) with ACSF in an interface chamber maintained at 25°C. Field recordings of the Schaffer collateral synapse were monitored for a minimum of 10 min before recording to insure a stable baseline. Responses are presented as an average of 6 individual traces. Baseline stimulus intensities were determined from the stimulus intensity required to produce a population EPSP at 50% of the maximal response. LTP was induced with two trains of 100 Hz stimulation for 1 s, separated by 20 s (indicated by an arrow, Figures 4B, 4D, and 4F), with the identical stimulus intensity used for baseline recordings.

Cerebellar Slice Physiology

Sagittal cerebellar slices of 200–250 μm thickness were prepared from the wild-type (P45–P79, n = 4) and *Sca1*$^{154Q/2Q}$ (P46–P78, n = 4) mice as described previously (Aiba et al., 1994; Kano et al., 1997). Whole-cell recording was made from visually identified Purkinje cells using a 40× water immersion objective attached to an upright microscope (Olympus, BX-50WI) (Edwards et al., 1989). Resistance of patch pipettes was 3–6 MΩ when filled with an intracellular solution composed of: 60 mM CsCl, 10 mM Cs D-gluconate, 20 mM TEA-Cl, 20 mM BAPTA, 4 mM $MgCl_2$, 4 mM ATP, 0.4 mM GTP, and 30 mM HEPES, ([pH 7.3], adjusted with CsOH). The composition of standard bathing solution was: 125 mM NaCl, 2.5 mM KCl, 2 mM $CaCl_2$, 1 mM $MgSO_4$, 1.25 mM NaH_2PO_4, 26 mM $NaHCO_3$, and 20 mM glucose, which was bubbled continuously with a mixture of 95% O_2 and 5% CO_2. Bicuculline (10 μM) was always present in the saline to block spontaneous inhibitory postsynaptic currents. Ionic currents were recorded with a patch-clamp amplifier (Axopatch-1D, Axon Instruments). Stimulation and online data acquisition were performed using the PULSE software (HEKA, Germany). The signals were filtered at 3 kHz and digitized at 20 kHz. Fitting of the decay phases of EPSCs was done with the PULSE-FIT software (HEKA, Germany). For stimulation of climbing fibers and parallel fibers, a glass pipette with a 5–10 μm tip diameter filled with standard saline was used. Square pulses (duration, 0.1 ms; amplitude, 0–100 V for climbing fiber stimulation, 1–10 V for parallel fiber stimulation) were applied for focal stimulation.

Immunohistochemistry and Immunofluorescence

Immunohistochemical and immunofluorescence staining were performed as previously described elsewhere (Skinner, et al., 1997; Cummings et al., 1999). The following antisera were used to stain brain tissue: rabbit polyclonal anti-ataxin-1 (11NQ), monoclonal anti-HDJ2/HSDJ (1:200, Neomarkers), monoclonal anti-ubiquitin (1:200, Novo Castra), and monoclonal anti-calbindin (1:1000, Sigma). For the quantitation of dendritic arborization, sections 20 μm thick or more were taken from of frozen fixed cerebelli of control and *Sca1*$^{154Q/2Q}$ mice at 19 weeks of age. Samples were matched to minimize processing variations within each group. Sections were stained with anti-calbindin antibody which lables all cytoplasmic regions of purkinje cells. After washing and mounting in Vectashield, 37 0.5 μm optical sections were accumulated with a Biorad 1024 confocal microscope using the same parameters for each sample. The brightest continuous series of 30 sections was projected using the NIH Image J zprojection routine set for average intensity. From the resulting 15 μm optical slabs, a rectangular subsection of a cerebellar hemi-folium was selected from the same region and same folium of each sample. The fluorescence intensiy profile of this slab was calculated using the plot profile routine of Image J and the resulting data used to develop comparative fluorescence intensity and average change in intensity over the course of the cell dendritic arbor.

Cell Counting

Midsagittal brain sections were prepared from 40-week-old *Sca1*$^{154Q/2Q}$ mice and age-matched controls (n = 3, for each group). After HE staining, the number of Purkinje cells and hippocampal pyramidal neurons in two to four adjacent sections from each brain was counted under light microscopy and averaged. Statistical analysis was carried out with ANOVA.

Acknowledgments

We thank Dr. Hannes Vogel and Michael Fernandez for expert technical assistance and V. Brandt for a critical reading of the manuscript. This work is supported by grants from the National Institute of Neurological Disorders and Stroke of the NIH to H.Y.Z. (NS27699) and H.T.O. (NS22920) and by cores from the Mental Retardation Research Center at Baylor College of Medicine. H.Y.Z. is an Investigator and K.W. is a Postdoctoral Research Associate with the Howard Hughes Medical Institute.

Received: November 16, 2001
Revised: May 7, 2002

References

Aiba, A., Kano, M., Chen, C., Stanto, M.E., Fox, G.D., Herrup, K., Zwingman, T.A., and Tonegawa, S. (1994). Deficient cerebellar long-term depression and impaired motor learning in mGluR1 mutant mice. Cell *79*, 377–388.

Bürk, K., Bösch, S., Globas, C., Zühlke, C., Daum, I., Klockgether, T., and Dichgans, J. (2001). Executive dysfunction in spinocerebellar ataxia type 1. Eur. Neurol. *46*, 43–48.

Burright, E.N., Clark, H.B., Servadio, A., Matilla, T., Feddersen, R.M., Yunis, W.S., Duvick, L.A., Zoghbi, H.Y., and Orr, H.T. (1995). SCA1 transgenic mice: a model for neurodegeneration caused by an expanded CAG trinucleotide repeat. Cell *82*, 937–948.

Clark, H.B., Burright, E.N., Yunis, W.S., Larson, S., Wilcox, C., Hartman, B., Matilla, A., Zoghbi, H.Y., and Orr, H.T. (1997). Purkinje cell expression of a mutant allele of SCA1 in transgenic mice leads to disparate effects on motor behaviors, followed by a progressive cerebellar dysfunction and histological alterations. J. Neurosci. *17*, 7385–7395.

Cummings, C.J., Mancini, M.A., Antalffy, B., DeFranco, D.B., Orr, H.T., and Zoghbi, H.Y. (1998). Chaperone suppression of aggregation and altered subcellular proteasome localization imply protein misfolding in SCA1. Nat. Genet. *19*, 148–154.

Cummings, C.J., Reinstein, E., Sun, Y., Antalffy, B., Jiang, Y., Ciechanover, A., Orr, H.T., Beaudet, A.L., and Zoghbi, H.Y. (1999). Mutation of the E6-AP ubiquitin ligase reduces nuclear inclusion frequency while accelerating polyglutamine-induced pathology in SCA1 mice. Neuron *24*, 879–892.

Cummings, C.J., Sun, Y., Opal, P., Antalffy, B., Mestril, R., Orr, H.T., Dillman, W.H., and Zoghbi, H.Y. (2001). Over-expression of inducible HSP70 chaperone supresses neuropathology and improves motor function in SCA1 mice. Hum. Mol. Genet. *10*, 1511–1518.

Edwards, F.A., Konnerth, A., Sakmann, B., and Takahashi, T. (1989). A thin slice preparation for patch-clamp recordings from neurons of the mammalian central nervous system. Pflugers Arch. *414*, 600–612.

Fernandez-Funez, P., Nino-Rosales, M.L., de Gouyon, B., She, W.-C., Luchak, J.M., Martinez, P., Turiegano, E., Benito, J., Capovilla, M., Skinner, P.J., et al. (2000). Identification of genes that modify ataxin-1-induced neurodegeneration. Nature *408*, 101–106.

Frankland, P.W., Cestari, V., Filipkowski, R.K., McDonald, R.J., and Silva, A.J. (1998). The dorsal hippocampus is essential for context discrimination but not for contextual conditioning. Behav. Neurosci. *112*, 863–874.

Genis, D., Matilla, T., Volpini, V., Rossel, J., Davalos, A., Ferrer, I., Molins, A., and Estivill, X. (1995). Clinical, neuropathologic, and genetic studies of a large spinocerebellar ataxia type 1 (SCA1) kindred: (CAG)n expansion and early premonitory signs and symptoms. Neurology *45*, 24–30.

Gusella, J.F., and MacDonald, M.E. (2000). Molecular genetics: unmasking polyglutamine triggers in neurodegenerative disease. Nat. Rev. Neurosci. *1*, 109–115.

Jiang, Y.H., Armstrong, D., Albrecht, U., Atkins, C.M., Noebels, J.L., Eichele, G., Sweatt, J.D., and Beaudet, A.L. (1998). Mutation of the Angelman ubiquitin ligase in mice causes increased cytoplasmic p53 and deficits of contextual learning and long-term potentiation. Neuron *21*, 799–811.

Kano, M., Hashimoto, K., Kurihara, H., Watanabe, M., Inoue, Y., Aiba, A., and Tonegawa, S. (1997). Persistent multiple climbing fiber innervation of cerebellar Purkinje cells in mice lacking mGluR1. Neuron *18*, 71–79.

Kish, S.J., el Awar, M., Schut, L., Leach, L., Oscar Berman, M., and Freedman, M. (1988). Cognitive deficits in olivopontocerebellar atrophy: implications for the cholinergic hypothesis of Alzheimer's dementia. Ann. Neurol. *24*, 200–206.

Klement, I.A., Skinner, P.J., Kaytor, M.D., Yi, H., Hersch, S.M., Clark, H.B., Zoghbi, H.Y., and Orr, H.T. (1998). Ataxin-1 nuclear localization and aggregation: role in polyglutamine-induced disease in SCA1 transgenic mice. Cell *95*, 41–53.

Kuemmerle, S., Guntekunst, C.A., Klein, A.M., Li, X.J., Li, S.H., Beal, M.F., Hersch, S.M., and Ferrante, R.J. (1999). Huntington aggregates may not predict neuronal death in Huntington's disease. Ann. Neurol. *46*, 842–849.

Llano, I., Marty, A., Armstrong, C.M., and Konnerth, A. (1991). Synaptic- and agonist-induced excitatory currents of Purkinje cells in rat cerebellar slice. J. Physiol. (Lond.) *434*, 183–213.

Lin, C.-H., Tallaksen-Greene, S., Chien, W.-M., Cearly, J.A., Jackson, W.S., Crouse, A.B., Ren, S., Li, X.-J., Albin, R.L., and Detloff, P.J. (2001). Neurological abnormalities in a knock-in mouse model of Huntington's disease. Hum. Mol. Genet. *10*, 137–144.

Lin, X., Cummings, C.J., and Zoghbi, H.Y. (1999). Expanding our understanding of polyglutamine diseases through mouse models. Neuron *24*, 499–502.

Lin, X., Antalffy, B., Kang, D., Orr, H.T., and Zoghbi, H.Y. (2000). Polyglutamine expansion down-regulates specific neuronal genes before pathologic changes in SCA1. Nat. Neurosci. *3*, 157–163.

Logue, S.F., Paylor, R., and Wehner, J.M. (1997). Hippocampal lesions cause learning deficits in inbred mice in the Morris water maze and conditioned fear task. Behav. Neurosci. *111*, 104–113.

Lorenzetti, D., Watase, K., Xu, B., Matzuk, M.M., Orr, H.T., and Zoghbi, H.Y. (2000). Repeat instability and motor incoordination in mice with a targeted expanded CAG repeat in the Sca1 locus. Hum. Mol. Genet. *9*, 779–785.

Matilla, A., Roberson, E.D., Banfi, S., Morales, J., Armstrong, D.L., Burright, E.N., Orr, H.T., Sweatt, J.D., Zoghbi, H.Y., and Matzuk, M.M. (1998). Mice lacking ataxin-1 display learning deficits and decreased hippocampal paired-pulse facilitation. J. Neurosci. *18*, 5508–5516.

McCampbell, A., Taylor, J.P., Taye, A.A., Robitschek, J., Li, M., Walcott, J., Merry, D., Chai, Y., Paulson, H., Sobue, G., and Fischbeck, K.H. (2000). CREB-binding protein sequestration by expanded polyglutamine. Hum. Mol. Genet. *9*, 2197–2202.

McLean, C.A., Cherny, R.A., Fraser, F.W., Fuller, S.J., Smith, M.J., Beyreuther, K., Bush, A.I., and Masters, C.L. (1999). Soluble pool of Aβ amyloid as a determinant of severity of neurodegeneration in Alzheimer's disease. Ann. Neurol. *46*, 860–866.

Muchowski, P.J., Ning, K., D'Souza-Schorey, C., and Fields, S. (2002). Requirement of an intact microtubule cytoskeleton for aggregation and inclusion body formation by a mutant huntingtin fragment. Proc. Natl. Acad. Sci. USA *99*, 727–732.

Nakamura, K., Jeong, S.Y., Uchihara, T., Anno, M., Nagashima, K., Nagashima, T., Ikeda, S., Tsuji, S., and Kanazawa, I. (2001). SCA17, a novel autosomal cerebellar ataxia caused by an expanded polyglutamine in TATA-binding protein. Hum. Mol. Genet. *10*, 1441–1448.

Nucifora, F.C., Jr., Sasaki, M., Peters, M.F., Huang, H., Cooper, J.K., Yamada, M., Takahashi, H., Tsuji, S., Troncoso, J., Dawson, V.L., et al. (2001). Interference by huntingtin and atrophin-1 with CBP-mediated transcription leading to cellular toxicity. Science *291*, 2423–2428.

Paylor, R., Tracy, R., Wehner, J., and Rudy, J.W. (1994). DBA/2 and C57BL/6 mice differ in contextual fear but not auditory fear conditioning. Behav. Neurosci. *108*, 810–817.

Roberson, E.D., and Sweatt, J.D. (1996). Transient activation of cyclic AMP-dependent protein kinase during hippocampal long-term potentiation. J. Biol. Chem. *271*, 30436–30441.

Servadio, A., Koshy, B., Armstrong, D., Antalffy, B., Orr, H.T., and Zoghbi, H.Y. (1995). Expression analysis of the ataxin-1 protein in tissues from normal and spinocerebellar ataxia type 1 individuals. Nat. Genet. *10*, 94–98.

Shimura, H., Schlossmacher, M.G., Hattori, N., Frosch, M.P., Trockenbacher, A., Schneider, R., Mizuno, Y., Kosik, K.S., and Selkoe, D.J. (2001). Ubiquitination of a new form of alpha-synuclein by parkin from human brain: implications for Parkinson's disease. Science *293*, 263–269.

Skinner, P.J., Koshy, B.T., Cummings, C.J., Klement, I.A., Helin, K., Servadio, A., Zoghbi, H.Y., and Orr, H.T. (1997). Ataxin-1 with an

expanded glutamine tract alters nuclear matrix-associated structures. Nature *389*, 971–974.

Steffan, J.S., Bodai, L., Pallos, J., Poelman, M., McCampbell, A., Apostol, B.L., Kazantsev, A., Schmidt, E., Zhu, Y.-Z., Greenwald, M., et al. (2001). Histone deacetylase inhibitors arrest polyglutamine-dependent neurodegeneration in Drosophila. Nature *413*, 739–743.

Telenius, H., Kremer, H.P.H., Theilmann, J., Andrew, S.E., Almqvist, E., Anvret, M., Greenberg, C., Greenberg, J., Lucotte, G., Squitieri, F., et al. (1993). Molecular analysis of juvenile Huntington disease: the major influence on (CAG)n repeat length is the sex of the affected parent. Hum. Mol. Genet. *2*, 1535–1540.

Walsh, D.M., Klyubin, I., Fadeeva, J.V., Cullen, W.K., Anwyl, R., Wolfe, M.S., Rowan, M.J., and Selkoe, D.J. (2002). Naturally secreted oligomers of amyloid β protein potently inhibit hippocampal long-term potentiation *in vivo*. Nature *416*, 535–539.

Zoghbi, H.Y., and Orr, H.T. (1995). Spinocerebellar ataxia type 1. Semin. Cell Biol. *6*, 29–35.

Zoghbi, H.Y., and Orr, H.T. (2000). Glutamine repeats and neurodegeneration. Annu. Rev. Neurosci. *23*, 217–247.